A Computerized System for Detection of Spiculated Margins based on Mammography

Qaisar Abbas[1], Irene Fondo´n[2], and Emre Celebi[3]
[1]College of Computer and Information Sciences, Al Imam Mohammad Ibn Saud Islamic University, Saudi Arabia
[2]Department of Signal Theory and Communications, School of Engineering Path of Discovery, Spain
[3]Department of Computer Science, Louisiana State University, USA

Abstract: *Spiculated margins indicate a high risk of malignancy for breast cancer. Detection accuracy of current computerized diagnostic systems Computer Aided Detections (CADs) for spiculated margins is not high due to the existence of intensity heterogeneities, often subtle and varied in appearance. This paper presents an automatic system for Accurately Detection of Spiculated Margins (ADSM) by measuring its physical properties. In proposed system, a pre-processing step is performed to suppress background noise and enhance contrast. Spiculated margins are then segmented by a Maximum Fuzzy Entropy Partitioning (MFEP) algorithm whose parameters are optimized using the Quantum Genetic Algorithm (QGA). Afterwards, the characterization of spicule regions is completed using morphological operators, Steerable-Ridge-Filtering (SRF) and quantification of physical properties. A data set of 220 mammogram masses was used to evaluate the proposed system. Experimental results indicate that the ADSM system achieves a high accuracy level of Area Under the receiver operating characteristics Curve (AUC): 0.875 compared to state-of-art systems. By integrating the ADSM system, the performance of CADs could potentially be improved.*

Keywords: *CAD, spiculated mass segmentation, image enhancement, fuzzy entropy, QGA, SRF.*

Received April 12, 2013; accepted March 17, 2014; published online December 3, 2014

1. Introduction

The American Cancer Society reported that 39, 620 [23] women were died due to breast cancer and 232, 340 new cases were diagnosed in the year of 2013. After lung cancer, it is the second leading cause of deaths. For early diagnosis, screening mammography [16] is widely considered as the most reliable and cost-effective method. The detection and interpretation of suspicious abnormalities in mammograms is a difficult task for radiologists. Therefore, Computer Aided Diagnostic systems (CADs) [2] for mammograms have been developed to characterize [11] masses into benign and malignant. The current CADs [18] consist of different stages such as segmentation of masses, detection of the spiculation levels, extraction of clusters of microcalcification and final mass classification. Among these stages, the detection of spiculation margins [19] is one of the most important features indicating a high risk of malignancy. However, the automatic detection of spiculation margins is a very difficult task for CADs.

To address this issue, several techniques [9, 13, 14, 20, 21, 22, 25] have been presented. For instance to detect spiculation mass, wavelet pyramid representation [12] method is used. Sampat *et al.* [20, 21, 22] measure the spiculation levels with some statistical characteristics such as spicule length, width-base, width-tip, major axis, minor axis and the number of spicules. An aggregated function is developed in [22] to combine statistical characteristics and then determine the mass spiculation levels. To achieve this detection, the plane fitting method is developed in [9]. Unfortunately, this method removes many important features such as microcalcification and even spicules. A semi-supervised multilevel learning based segmentation technique for spiculated masses is presented in [14].

The literature review shows that a significant research effort has been done for the development of segmentation methods for spiculated masses and the detection of spiculation levels. However, the design of an accurate and fast spicule detection system is still a challenging task due to the fact that spiculated margins are often subtle and varied in appearance.

In this paper, an optimized and Accurate Detection of Spiculated Margins (ADSM) system is proposed by measuring physical properties of the spiculation levels. The ADSM system consists of preprocessing, spiculated mass segmentation by optimization of fuzzy parameters, extraction of spiculated regions, detection of spiculated lines in those regions and computation of physical properties steps. In preprocessing step, a contrast limited adaptive histogram equalization method [1], gamma correction and gaussian filtering techniques are applied to enhance the background and to reduce the influence of noise for the selected Region-Of-Interests (ROI). Next, the spiculated mass

segmentation step is performed by using the Maximum Fuzzy Entropy Parti-Tioning (MFEP) technique of the 2D histogram. In general, the MFEP technique has also been used in several systems [4, 5, 6, 8, 15, 24, 27, 28]. By using the MFEP of the 2D image histogram, the lots of fuzzy subsets are generated, which are optimized using a Quantum Genetic Algorithm (QGA). Usually for parameters optimization, Genetic Algorithm (GA) [13] is mostly utilized but QGA is more convenient and efficient when solving optimization problems in many applications [12, 17, 26] especially in image segmentation [10]. In ADSM system, QGA algorithm has been adopted because spiculated masses have intensity heterogeneities and irregular or fuzzy borders. Due to these reasons, QGA with MFEP based segmentation methods are used to provide an effective segmentation solution. To detect the spiculated region in the segmented area, morphological functions are used.

In the next step, Gaussian Steerable Filtering (GSF) [7] is utilized. This GSF technique is extended to develop a Steerable Ridge Filtering (SRF) method that can effectively segment spicule lines. Afterwards, the mass spiculation levels are quantified by measuring the physical characteristics of spicule lines. To test the performance of ADSM system, a data set of 220 mammogram masses is used that obtained from Digital Database for Screening Mammography (DDSM) [3]. To assess accuracy level of the ADSM system, Area Under the receiver operating characteristics Curve (AUC) technique is used with 95% confidence level. Furthermore, the comparisons with state-of-the-art techniques such as spiculated mass detection by Jiang *et al*. [9, 21] are performed.

The remainder of the paper is organized as follows. In section 2, the proposed ADSM system is described in detail with selected dataset. In section 3, the experimental results are presented. Finally, discussion, conclusions and recommendations for future work are given in section 4.

2. Materials and Methods

2.1. Data Set

The performance of the proposed ADSM system is evaluated on 220 ROI images from selected mammograms obtained from DDSM [3]. This DDSM dataset contains 2,620 study cases, but we have selected images that contain spiculated and non-spiculated masses. In DDSM dataset, the images are stored using lossless JPEG compression format. Each mammogram image has a large size due to the scanning resolution (between 42 and 100 microns). To uncompress these images and to reduce size of each image, the software provided by michael heath of the USF Computer Vision Laboratory has been used. After that these images are sub-sampled by an average value of (8×8) window and the size of (300×300) pixels is selected from each sub-sampled image.

2.2. Methods

2.2.1. Pre-Processing

In this step, the contrast of the ROI image is enhanced by utilizing a technique developed in [1]. Abbas *et al*. [1] used a histogram equalization, gamma correction and gaussian filtering methods to develop a contrast enhancement solution without affecting breast mass features and after applying the enhancement technique [1], the contrast is more cleared compare to surrounding areas of the ROI image. For detailed implementation, Abbas *et al*. [1] are requested to study the description of this contrast enhancement technique in the paper.

2.2.2. Spiculated Mass Segmentation

After preprocessing step, the MFPE [24] procedure is used for segmentation of spiculated mass, with its fuzzy parameters optimized through a QGA [10]. The MFPE technique is applied to select the threshold value to segment the grayscale mammograms in an optimized framework. The MFPE segmentation technique is divided image into fuzzy pixels of three classes of the form of Dark gray (D), Medium gray (M) and white (H) with a membership function Z-function, Π-function and S-function, respectively. Afterwards, the Total entropy (T(P)) for the 2D histogram of the fuzzy partition is calculated by adding the entropy of these member functions.

The T(P) can be regarded as a measure of the whole information for the 12 parameters of the grayscale image based on the fuzzy partition P={D, H, M}. Since, our aim is to find the maximum information based on a fuzzy partition, this algorithm is called MFPE. Therefore, the optimization process consists of searching for an optimal combination of 12 parameters such that the T(P) is maximized. According to this, the pixels can be classified into three classes based on the maximum membership principle: if $\mu_D(i, j) \geq 0.5$, the pixel is classified as belonging to the dark part D. If $\mu_M(i, j) \geq 0.5$, the pixel belongs to the medium gray part, otherwise it belongs to white part H. Due to large number of combinations of the 12 parameters in a multidimensional fuzzy partition; it is not feasible to evaluate each and every parameter configuration. Thus, a QGA is used to optimize these parameters QGA is based on quantum vectors representing chromosomes by qubit coding method, updating them by a quantum rotation gate. The best threshold is expressed by the binary numbers. It must be noticed that the process of encoding parameters into an alphabetic string has been performed same as explained in [26]. Some other QGA parameters have been empirically fixed such as maximum number of generations=1000, population

size=40 and dimension of parameters=12 such that qubit string (k =12×8=96).

By using MEFP and QGA based segmentation techniques, the three fuzzy regions are obtained. The white-segmented fuzzy area represents the spiculated mass and region. By performing a linear search method, this white-segmented region is detected. There are also some small irregular objects that could have high gradient intensity as the spiculated lines such as micro calcification. In the proposed ADSM system, we are interested in the detection of spiculated lines and therefore a simple technique based on morphological processing has been used to separate spiculated mass, and its surrounding region from the background. In the subsequent two sections, the detection detail about spiculated mass and region are described.

2.2.3. Spiculated Mass and Region Detection

MFEP and QGA techniques divide the ROI image into three groups according to the gray level of the pixels. The detection of Spiculated Mass and Region Detection (SMRD) step is carried out based on the group of white pixels in this ADSM system. Two types of information are considered by the SMRD process: Spiculated-Mass Area (SMA) showing high gradient information across boundary points, and the Maximum Spiculated-Area (MSA) around the corresponding spiculated mass boundary. We extracted SMA through optimal searching of spiculated lines in the ROI image. To detect SMRD regions, a morphological reconstruction functions is used to the white group of pixels. Morphol-ogical operators are used in many different fields such as MRI image segmentation [8] so these are adopted for the final segmentation of spiculated mass and region.

To segment the SMA, morphological area-opening and hole-filling operations are utilized. With the area-opening function the algorithm removes from white-pixels group image all connected components that have fewer than P_{obj} pixels based on 8-connectivity. Let C_c be the connected components defined for image $B(i, j)$, S be the area of each C_c component, smaller objects are filtered as follows:

$$f(i,j)=\begin{Bmatrix} B(i,j) & if\ area(S)\geq P_{obj} \\ 0 & otherwise \end{Bmatrix} \quad (1)$$

To avoid holes in the detected area of $f(i, j)$ image, the hole-filling function is applied as follows:

$$f'(i,j)=\begin{Bmatrix} f(i,j)+255 & if\ surrounding\_area(f(i,j))=255 \\ 0 & otherwise \end{Bmatrix} \quad (2)$$

MSA is also obtained by morphology: Area-opening, dilation and hole-filing functions. After getting $f(i, j)$ image, dilation is applied based on the circular structuring element S_E of radius 9 pixels domain D_{S_E}, which is given by:

$$(f \otimes S_E)(i,j)=max\left\{f(i-i',j-j') \mid (i',j')\in D_{S_E}\right\} \quad (3)$$

However, the final MSA region is obtained by adding the area segmented by morphological function and 40 pixels around that area. Finally, the two segmented regions, SMA and MSA are superimposed on the contrast enhanced ROI image. Actually, SMA describes the spiculated mass segmentation step and MSA area is subsequently used to detect the maximum detection area of the location of spiculated lines. To attain improve accuracy; the spicule lines are segmented from inside SMA up to boundary of MSA.

2.2.4. Detection of Spiculated-Lines and Level

After identifying spiculated mass and region, the detection of spiculated lines and level step is performed. There are some linear structures within the spiculated lesion and the surrounding region that describe spiculated lines. To extract the spicules, a new linear structure or ridge detection filter is proposed based on the gaussian steerable filter, i.e., Steerable Ridge Filter (SRF). The SRF filtering provides the advantage of steerability to enhance, while detecting the linear structures.

Let $M_{sp}(x, y)$ be the maximum spiculated region segmented from the previous step. Then, the second derivative of Gaussian-smooth steerable filer is given by:

$$g_\phi(x,y;\phi)=((x^2\phi-\sigma^2\phi)(y^2\phi-y^2\phi))/2\pi\sigma^2 exp\left(-(x^2\phi+y^2\phi)/(\sigma^2\phi)\right) \quad (4)$$

It has the separability property so we can obtain:

$$R(x)=\max_{\sigma,\phi}\left\{g_\phi(\sigma(x);\phi)\otimes M_{sp}(x)\right\} \quad (5)$$

And

$$R(y)=\max_{\sigma,\phi}\left\{g_\phi(\sigma(y);\phi)\otimes M_{sp}(y)\right\} \quad (6)$$

Where σ and ϕ are the scale and the orientation of the detected lines in both x and y direction, respectively and $\otimes$ denotes convolution operation. The ϕ varies from 0 to 2π such that:

$$E_{map}(x',y')=cos\phi\times R(x)+sin\phi\times R(y) \quad (7)$$

The $E_{map}(x', y')$ edge map effectively detects spiculated lines in all directions, but there are also some blood vessels, which are thicker than spiculated lines that are also detected by Equation 7. Therefore, to separate these thicker lines, first a gaussian filtering operation with a weight towards the centre of the detected spiculated region $M_{sp}(x, y)$ is performed, which is defined as:

$$B_{map}(x',y')=cos\left(\frac{\pi x}{2\alpha}\right)\times cos\left(\frac{\pi y}{2\alpha}\right)exp\left(-(x^2+y^2)/(2\alpha)\right) \quad (8)$$

Where α is a fixed parameter with a value of 0.5. Therefore, from the extracted lines from $E_{map}(x', y')$ edge map, the algorithm discards all lines from $B_{map}(x', y')$ of Equation 8.

$$Lines_{sp}(x,y) = E_{map}(x',y') - B_{map}(x',y') \quad (9)$$

However, this procedure might detect blob like structures such as spiculated mass boundary lines. To avoid this situation, mass contour pixels are extracted from Equation 1 in the canny edge map and compared it pixel-by-pixel with $Lines_{sp}(x,y)$ function, which is described as follows:

$$Spicule_{SRF}(x,y) = \left\{ \begin{array}{ll} Lines_{sp}(x,y) & if\ any\ pixel\ of\ S_{lines}(x,y) \notin f_{canny\_edgemap}(x,y) \\ 0 & otherwise \end{array} \right\} \quad (10)$$

These lines are provided an evidence for the presence of a spiculated mass. The spiculation levels of the mass are quantified by measuring various physical characteristics of the detected spicule: The spicule-length, spicule-width, spiculated-max (area), spiculated-min (area), major and minor axes and the number of spicules. Thus, we obtained:

$$Spiculation\_level(i) = \left\{ \begin{array}{l} Spicule\text{-}length, Spicule\text{-}width, \\ \qquad Spiculated\text{-}min(area), \\ \qquad Spiculated\text{-}max(area), \\ \qquad , Major\text{-}axis , Minor\text{-}axis \\ \qquad , Num\text{-}Spicule \end{array} \right\} \quad (11)$$

3. Experimental Results

The proposed ADSM system has been tested with the dataset obtained from the DDSM, which is the largest publicly available data set of digitized mammograms. To evaluate the performance of the algorithm, two sets of ROIs masses have been used from this data set. One set contained 110 spiculated ROI masses and the other contained 110 non-spiculated ROI masses from a total of 220 mammogram images. The experiments are performed on a 2.3GHz Core2 Duo 32bit Intel processor with 1GB DDR2 RAM. The ADSM system is implemented in MATLAB 7.6.0.324® (The Mathworks, Natick, MA).

On average, 14.996 (s) are required in total for ADSM system to perform the steps on a (300×300) pixels ROI image. To differentiate between spiculated and non-spiculated masses, the physical measurements such as spicule-length, spicule-width, spiculated-min (area), spiculated-max (area), major-axis, minor-axis and num-spicule have been calculated. These properties are used to establish the spiculation levels, and subsequently to differentiate between spiculated, and non-spiculated masses. The higher the spiculation levels mean that the greater the risk of malignancy. To test the performance, the comparisons from ADSM system with state-of-the-art systems such as Jiang *et al*. [9, 21] are also performed. Figures 1-a, b and c visually represents results of the three ROI images by using ADSM, SampatSL and JiangSL systems, respectively. From this figure, the ADSM system is accurately detected every type of spiculated lines (thick and thin) compared to other two systems. Moreover, the average and standard deviation of measurement properties of the 110 spiculated masses and 110 non-spiculated masses are also calculated. In general, the measurements of spiculated mass regions are higher than those of other mass regions. In this data set, the average spicule-length, spicule-width and num-spicule values for the 110 spiculated masses are 12.4, 2.4 and 176.4, while those of 110 other masses are all zeros, respectively.

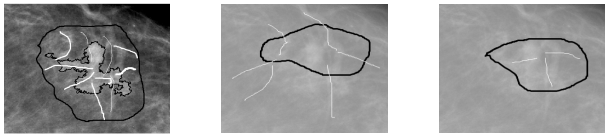

a) Proposed ADSM. b) SampatSL [21]. c) JiangSL [9] systems.

Figure 1. Some of the results obtained from spiculated mass segmentation and line detection systems.

When a threshold (0.5 or 95% confidence interval) is applied to simply classify between the groups containing spiculated and non-spiculated mass regions by using physical properties of spicules, 84.2% rate of correct classification is obtained with 82.2% sensitivity and 92.85% specificity. To show this performance on the 220 ROI spiculated masses, we have computed the ROC curve as shown in Figure 2. It shows the overall performance of this ADSM system is also effectively distinguished between spiculated and non-spiculated mass regions. The computed area under the ROC curve AUC value is 0.875. As a result, the proposed system is highly accurate for measuring the spiculation margins. Due to use of fuzzy entropy, QGA and morphological edge detection techniques, our computer-based system is reliable segmented the maximum spiculated area and spiculated mass. The proposed spiculated line detection algorithm is effectively segmented the spiculated lines than blood vessels. Furthermore, the developed system is focused on more physical properties of measuring the spiculation levels compared to other techniques.

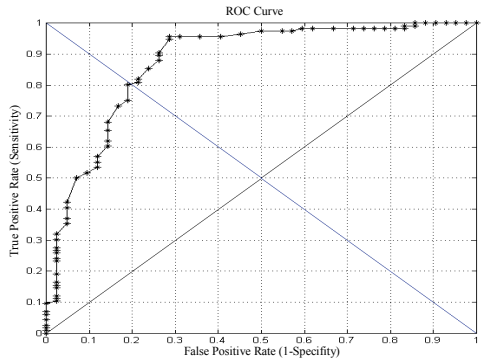

Figure 2. Receiver-operating characteristic curve for distinguishing between spiculated and non-spiculated mass regions.

4. Discussions and Conclusions

Mass spiculation levels are widely recognized feature for the classification of mammographic masses. It is also a very important index of malignancy for breast cancer. Thus, the detection of spiculated mass regions has attracted substantial research interest in the past.

The literature review suggests that the detection accuracy of spiculated masses is approximately 72%, which is not satisfactory possibly due to the difficulty of spiculated mass segmentation, intensity heterogeneities, ill-defined and fuzzy borders, tissue noise, and similarity of spicules and blood vessels, which reduces the detection accuracy. The proposed ADSM computerized system is an effective spiculated mass and level detection system with the following unique features compared to existing techniques. A new ill-defined and fuzzy spiculated mass segmentation algorithm is developed using fuzzy entropy and GA that can reliable segment spiculated area of mass. This segmentation algorithm is outperformed than state-of-the-art mass segmentation techniques. It increases the detection accuracy of mass spiculation levels from 72% to more than 85% due to use of robust segmentation technique and a new steerable line detection algorithm. The main advantage of our proposed spiculated line detection algorithm as compared to other methods is that it is effectively segment the spiculated lines than blood vessels. The developed system is focused on more physical properties of measuring the spiculation levels compared to other techniques. As a result, it increases the performance level of mammography CAD systems.

In different type of mammographic masses, the spiculated mass regions are accurately detected. But, it might be possible that if spiculated mass is highly surrounding by breast dense tissue and blood vessels then our segmentation algorithm may not detect proper boundary of mass. Other limitation of this algorithm is that the preprocessing step may enhance all linear structures, with similar width to those of spicules. Another limitation of the current study is that the measurements were made on a small number of cases, and thus we are planning increase the data set size to better tune our algorithm. We strongly believe that the systematic study and quantification of the physical parameters of spiculation levels would be used by many future researchers in CAD systems.

Acknowledgements

This study is supported by the COMSTAS Institute of Information Technology and Higher Education Commission (HEC) of Pakistan with grant no. PM-IPFP/HRD/HEC/2010/2395.

References

[1] Abbas Q., Celebi M., and García I., "Breast Mass Segmentation using Region-Based and Edge-Based Methods in a 4-Stage Multiscale System," *Biomedical Signal Processing and Control*, vol. 8, no. 2, pp. 204-214, 2013.

[2] Bellotti R., De Carlo F., Tangaro S., Gargano G., Maggipinto G., Castellano M., Massafra R., Cascio D., Fauci F., Magro R., Raso G., Lauria A., Forni G., Bagnasco S., Cerello P., Zanon E., Cheran S., Lopez Torres E., Bottigli U., Masala G., Oliva P., Retico A., Fantacci M., Cataldo R., De Mitri I., and De Nunzio G., "A Completely Automated CAD System for Mass Detection in A Large Mammographic Database," *Medical Physics*, vol. 33, no. 8, pp. 3066-3075, 2006.

[3] Bowyer K., Kopans D., Kegelmeyer P., and Moore R., "The Digital Database for Screening Mammography," *in Proceedings of the 3rd International Workshop on Digital Mammography*, *International Congress Series*, Chicago, USA, pp. 432-434, 1996.

[4] Chen Z., Qiu T., and Ruan S., "A Segmentation Algorithm for Brain MR Images using Fuzzy Model and Level Sets," *International Journal of Innovative Computing Information and Control*, vol. 6, no. 12, pp. 5565-5574, 2010.

[5] Cheng H. and Chen J., "Automatically Determine the Membership Function based on the Maximum Entropy Principle," *Information Sciences*, vol. 96, no. 3, pp. 163-182, 1997.

[6] Cheng H., Chen J., and Li J., "Thresholding Selection Based on Fuzzy C-Partition Entropy Approach," *Pattern Recognition*, vol. 31, no. 7, pp. 857-870, 1998.

[7] Freeman W. and Adelsonk E., "The Design and Use of Steerable Filters," *IEEE Transactions on Pattern Analysis and Machine Intelligence*, vol. 13, no. 9, pp. 891-906, 1991.

[8] Jaffar M., Hussain A., and Mirza A., "Fuzzy Entropy and Morphology based Fully Automated Segmentation of Lungs From CT Scan Images," *International Journal of Innovative Computing Information and Control*, vol. 5, no. 12, pp. 4993-5002, 2009.

[9] Jiang L., Song E., Xu X., Ma G., and Zheng B., "Automated Detection of Breast Mass Spiculation Levels and Evaluation of Scheme Performance," *Academic Radiology*, vol. 15, no. 12, pp. 1534-1544, 2008.

[10] Laboudi Z. and Chikhi S., "Comparison of Genetic Algorithm and Quantum Genetic Algorithm," *the International Arab Journal of Information Technology*, vol. 9, no. 3, pp. 243-249, 2012.

[11] Lesniak J., Hupse R., Blanc R., Karssemeijer N., and Székely G., "Comparative Evaluation of Support Vector Machine Classification for Computer Aided Detection of Breast Masses in Mammography," *Physics in Medicine Biology*, vol. 57, no. 16, pp. 5295-5307, 2012.

[12] Li B. and Wang L., "A Hybrid Quantum-Inspired Genetic Algorithm for Multiobjective Flow Shop Scheduling," *IEEE Transactions on Systems Man and Cybernetics*, vol. 37, no. 3, pp. 576-591, 2007.

[13] Li F., Jin C., and Shi Y., "Fuzzy Programming Theory Based on Synthesizing Effect and Its Application," *International Journal of Innovative Computing Information and Control*, vol. 6, no. 8, pp. 3563-3572, 2010.
[14] Liu S., Babbs C., and Delp E., "Multiresolution Detection of Spiculated Lesions in Digital Mammograms," *IEEE Transaction on Image Processing*, vol. 10, no. 6, pp. 874-884, 2001.
[15] Luca A. and Termini S., "A Definition of Nonprobabilistic Entropy in the Setting of Fuzzy Set Theory," *Information and Control*, vol. 20, no. 4, pp. 301-312, 1972.
[16] Maurice A., Evans D., Affen J., Greenhalgh R., Duffy S., and Howell A., "Surveillance of Women at Increased Risk of Breast Cancer using Mammography and Clinical Breast Examination: Further Evidence of Benefit," *International Journal of Cancer*, vol. 131, no. 2, pp. 417-425, 2012.
[17] Nedjah N., Araujo M., and Mourelle L., "Quantum-Inspired Evolutionary Design of Synchronous Finite State Machines: Part 2," *International Journal of Innovative Computing Information and Control*, vol. 6, no. 11, pp. 4897-4910, 2010.
[18] Oliver A., Freixenet J., Martí J., Pérez E., Pont J., Denton E., and Zwiggelaar R., "A Review of Automatic Mass Detection and Segmentation in Mammographic Images," *Medical Image Analysis*, vol. 14, no. 2, pp. 87-110, 2010.
[19] Rawashdeh M., Bourne R., Ryan E., Lee W., Pietrzyk M., Reed W., Borecky N., and Brennan P., "Quantitative Measures Confirm the Inverse Relationship between Lesion Spiculation and Detection of Breast Masses," *Academic Radiology*, vol. 20, no. 5, pp. 576-580, 2013.
[20] Sampat M., Bovik A., Whitman G., and Markey M., "A Model-Based Framework for the Detection of Spiculated Masses on Mammography," *Medical Physics*, vol. 35, no. 5, pp. 2110-2123, 2008.
[21] Sampat M., Whitman G., Markey M., and Bovik A., "Evidence-Based Detection of Spiculated Masses and Architectural Distortions," available at: http://proceedings.spiedigitallibrary.org/proceeding.aspx?articleid=1281797, last visited 2013.
[22] Sampat M., Whitman G., Stephens T., and Broemeling L., "The Reliability of Measuring Physical Characteristics of Spiculated Masses on Mammography," *British Journal of Radiology*, vol. 79, no. 2, pp. 134-140, 2006.
[23] Siegel R., Naishadham D., and Jemal A., "Cancer Statistics, 2013," *CA: A Cancer Journal for Clinicians*, vol. 63, no. 1, pp. 11-30, 2013.
[24] Tao W., Tian J., and Liu J., "Image Segmentation by Three-Level Thresholding based on Maximum Fuzzy Entropy and Genetic Algorithm," *Pattern Recognition Letter*, vol. 24, no. 16, pp. 3069-3078, 2003.
[25] Tao Y., Lo S., Freedman M., Makariou E., and Xuan J., "Multilevel Learning-Based Segmentation of ill-Defined and Spiculated Masses in Mammograms," *Medical Physics*, vol. 37, no. 11, pp. 5993-6002, 2010.
[26] Xia J., Yan Y., Zhang J., and Tanga Y., "A Quantum-Inspired Genetic Algorithm for K-Means Clustering," *Expert Systems with Applications*, vol. 37, no. 7, pp. 4966-4973, 2010.
[27] Zadeh L., "Outline of a New Approach to the Analysis of Complex Systems and Decision Processes," *IEEE Transactions on Systems Man and Cybernetics*, vol. 3, no. 1, pp. 28-44, 1973.
[28] Zhao M., Fu A., and Yan H., "A Technique of Three-Level Thresholding based on Probability Partition and Fuzzy 3-Partition," *IEEE Transactions on Fuzzy Systems*, vol. 9, no. 3, pp. 469-479, 2001.

Qaisar Abbas received his BSc degree in computer science from the Bahauddin Zakaryia University (BZU), Pakistan, in 2001. He received his MSc in computer science from BZU and Doctor of engineering degree PhD from the University of HUST at (Wuhan, China) in 2004 and 2011, respectively. He was working as a software manager under Business Craft company (Spanish), which provided IT solutions from 2004-2009 and also as a lecture from 2006-2008 in the same University, where he did masters. From 2011 to 2013, he worked as an assistant professor at National Textile University, Faisalabad, Pakistan and after that he joined COMSATS for 1 and half years. Currently, he is working as an assistant professor at College of Computer and Information Sciences, Al Imam Mohammad Ibn Saud Islamic University (IMSIU), Riyadh, Saudi Arabia. His research interests include: image processing, medical image analysis, Genetic programming and pattern classification.

Irene Fondo´n received the MS degree in telecommunication engineering from the University of Seville, Spain, in 2004. She has completed her PhD degree in the year of 2011. She has been working as an associated professor since 2005 in the Signal Processing and Communications Department of the University of Seville. Her current research activities include works in the field of image processing and its medical applications. She is author of papers both in Journals and International Conferences.

Emre Celebi received his BSc degree in computer engineering from Middle East Technical University, Turkey in 2002, MSc and PhD degrees in computer science and engineering from the University of Texas at Arlington (Arlington, TX, USA) in 2003 and 2006, respectively. He is currently an associate professor in the Department of Computer Science at Louisiana State University, Shreveport, LA, USA). His research interests include medical image analysis, color image processing, content-based image retrieval, and open-source software development.